A. Fuentes, G. Legros, S. Rouvreau, P. Joulain, J.P. Vantelon, J.L. Torero and A.C. Fernandez-Pello, *Sooting Behaviour Dynamics of a Non-Bouyant Laminar Diffusion Flame*, Combust. Sci. and Tech. 179 (2007) 3-19.

SOOTING BEHAVIOUR DYNAMICS OF A NON-BUOYANT LAMINAR DIFFUSION FLAME

A. Fuentes[1,†], G. Legros[2], S. Rouvreau[1], P. Joulain[1], J.-P. Vantelon[1], J. L. Torero[3] and A.C. Fernandez-Pello[4]

[1] Laboratoire de Combustion et de Détonique
UPR 9028 du CNRS - Poitiers (FRANCE)
[2] Laboratoire de Mécanique Physique
Université Paris VI, Saint-Cyr l'Ecole, 78210, (FRANCE)
[3] School of Engineering and Electronics
The University of Edinburgh, Edinburgh (UNITED KINGDOM)
[4] Department of Mechanical Engineering
University of California, Berkeley, CA 94720 (USA)

[†] corresponding author:
Laboratoire de Combustion et de Détonique
1, av. C. Ader, BP 40109
86961 Chasseneuil-Futuroscope Cedex
FRANCE
fax: 00 33 5 49 49 82 91
email: andres.fuentes@lcd.ensma.fr

Abstract

Local soot concentrations in non-buoyant laminar diffusion flames have been demonstrated to be the outcome of two competitive processes, soot formation and soot oxidation. It was first believed that soot formation was the controlling mechanism and thus soot volume fractions could be scaled with a global residence time. Later studies showed that this is not necessarily the case and the local ratio of the soot formation and oxidation residence times is the prime variable controlling the ultimate local soot volume fractions. This ratio is a strong function of geometry and flow field, thus a very difficult variable to properly quantify. This study presents a series of microgravity, low oxidizer flow velocity, experiments where soot volume fraction measurements have been conducted on a laminar, flat plate boundary layer type diffusion flame. The objective of the study is to determine if the above observations apply to this type of diffusion flames. The fuel is ethylene and is injected through a flat plate porous burner into an oxidizer flowing parallel to the burner surface. The oxidizer consists of different mixtures of oxygen and nitrogen, flowing at different velocities. These experiments have been complemented with numerical simulations that emphasize resolution of the flow field to simulate the trajectory of soot particles and to track their history from inception to oxidation. The results validate that local soot volume fractions are a function of the local formation and oxidation residence times and are not necessarily a function of the global residence time. For this particular geometry, an increase in oxidizer velocity leads to local acceleration that reduce the oxidation residence time leading to higher soot concentrations. It was also observed that the flames become longer as the flow velocity is increased in contrast with the reversed trend observed in flames at higher flow velocities. This result is important because it seems to indicate the presence of a maximum in the flame length and luminosity below those encountered in natural convection. The result would have implications for fire

safety in spacecrafts since the ambient gas velocities are below those observed in natural convection, and longer and more luminous flames represent a higher hazard.

Keywords:

diffusion flame

soot

microgravity

Shortened title:

Sooting in a non-buoyant laminar diffusion flame

Introduction

In microgravity and low velocity gas flows, due to the absence of natural convection, time scales associated with combustion processes are longer than in normal gravity and radiation can be the predominant mode of heat transfer due to the small heat transfer coefficient, even for small diffusion flames (Olson and T'ien, 2000). Soot production is enhanced with increasing residence times, further emphasizing the role of radiation (Megaridis et al., 1996). Thus, a better understanding of soot formation and radiative emissions in microgravity diffusion flames is of importance to many practical combustion related processes and in particular in spacecraft fire safety (Olson and T'ien, 2000; Fernandez-Pello et al., 2000; Torero et al., 2002).

Several studies have attempted to describe the sooting behaviour of non-buoyant jet diffusion flames, notable are the studies by Faeth et coworkers (Lin et al., 1999; Lin and Faeth, 1999; Xu et al., 2002) and Konsur et coworkers (Megaridis et al., 1996; Konsur et al., 1999a,b). Underlying these studies is the Smoke-Point concept and the possibility of inferring the flame radiative losses only from the fuel flow rate. This concept was originally proposed by Markstein and De Ris (1984), for buoyant normal gravity flames, and suggests that the flame quenches due to radiative heat losses at a fixed soot concentration. Flames could be "closed-tip", if fuel is consumed before this critical concentration is attained, or "open-tip" if quenching occurs before the fuel is consumed. Flame lengths, and consequently other processes influenced by the flame length such as co-current flame spread, could then be linked to the critical soot concentration. Markstein and De Ris (1984) empirically verified this concept and alluded to the possibility of using the Smoke-Point as a material flammability criterion. Despite the utility of this approach, the question that remains unanswered is how the critical soot concentration for flame quenching is attained. Furthermore, for "open-tip"

flames, the flame length can only be determined if soot concentrations can be tracked along the reactive zone. An important issue that remains unresolved is the soot history. Local soot concentration will strongly depend on the history that precedes the arrival of soot to a specific location (Kennedy, 1997). Extensive effort has been devoted to soot formation and oxidation models that can predict local soot concentrations, but despite the numerous studies that have concentrated on soot formation in normal and microgravity many of the relevant processes are yet unclear and disagreement between models and theory is frequently reported. Discrepancies between models and experiments have been reported as early in the soot formation history as in the fuel entry nozzle, *i.e.* at the first soot appearance location. The origin of the error was attributed to improper far-field approximations and the effect that these have on the chemistry of soot formation (Xu et al., 2002). The disagreement is carried through the entire flame becoming most evident in the quenching region. Thus, models are still incapable of predicting the geometry of "open-tip" flames (Lin et al., 1999; Lin and Faeth, 1999; Xu et al., 2002).

Since soot production is the result of two competitive processes, formation and oxidation, defining the soot history requires detailed understanding of the mechanisms controlling these processes. Of critical importance is the effect of oxygen concentration on formation and oxidation, which links the soot history and local soot concentrations to the structure of the flow field in the proximity of the flame. The global residence time seems to be a key parameter controlling soot concentrations (Megaridis et al., 1996; Konsur et al., 1999b). Konsur et al. (1999b) determined that the peak soot volume fraction decreased when reducing the characteristic flow residence time. Mortazavi et al. (1993) demonstrated the capability to alter soot concentrations in non-buoyant laminar jet diffusion flames by varying the characteristic flow velocities.

Vietoris et al. (2000) and Brahmi et al. (2005) extended the above studies to a diffusion flame established in a non-buoyant laminar, flat plate, boundary layer. These authors focused on the visible emissions of the flame and showed that for low velocity air flows the luminosity of the flame increased with the oxidizer velocity for both solid (Vietoris et al., 2000) and gaseous (Brahmi et al., 2005) fuels. Luminous intensity can be correlated to the presence of soot, and its oxidation, in a high temperature region, and consequently to soot concentration. Therefore these observations can provide indirect evidence of the effect of the flow field on the competition between soot formation and oxidation. Legros et al. (2006) extended the above works to quantify the influence of the oxidizer velocity on soot concentrations showing that increasing the oxidizer velocity enhanced both soot oxidation and soot formation, with the latter dominating in the fuel injection region and the former near the flame trailing edge. In these experiments it was found that an increase in residence time leads to a decrease in the peak soot volume fraction, in contrast with the observations of Konsur et al. (1999b). Since in these studies the soot volume fraction fields are very different, they provide further evidence of the importance of the flow field on soot behaviour in diffusion flames. A subsequent numerical study proved that the orientation of the flow streamlines was at the origin of the observed changes in luminous intensity (Rouvreau et al., 2002) further ratifying the above statement.

To provide further evidence of the above observations, the present study focuses on the soot trajectory in a non-buoyant, laminar, flat plate, boundary layer diffusion flame similar to that of Brahmi et al. (2005). Experiments are conducted in microgravity using ethylene as fuel and a mixture of O_2 and N_2 as oxidizer. The parameters varied are fuel and oxidizer velocity. A numerical model to enable tracking the flow field and temperature of the soot particles complements the experimental measurements.

Experimental hardware

Figure 1 presents a schematic of the experimental apparatus, and of the burner with its relevant dimensions. A detailed description of the experimental apparatus can be found in Legros et al. (2006). The diffusion flame is established inside a 50 litre stainless steel combustion chamber, which has three large quartz windows for optical access. Confinement is required for safety in microgravity facilities, but all perturbations linked to confinement have been studied before, showing that the volume of the chamber is sufficient large to keep the flame free from wall effects. The pressure is kept at atmospheric by means of a differential pressure switch and proportional valve placed at the exhaust of the duct.

Ethylene is chosen as fuel for its well characterized sooting behaviour. It is injected via a mass flow controller through the porous square plate, which has a 50x50mm^2 effective section of injection. The oxidizer flow is introduced in the combustion chamber via mass flow controllers through a settling chamber and honeycomb plates. The oxidizer creates a boundary layer flow parallel to the burner surface where the diffusion flame is established. The oxidizer consists of a mixture of O_2 and N_2.

A 100mW green laser diode (λ=532nm) is used as a backlighting source to measure with an 8-bit monochrome and progressive CCD camera light attenuation through the flame (along the y axis on Fig. 1). More details on the experimental approach are given in Legros et al. (2006).

The microgravity experiments are conducted in parabolic flights that provide 22s long microgravity periods, and that have been proven sufficient to reach steady state in the flow and diffusion flame (Vietoris et al., 2000).

Experimental Results

An instantaneous greyscale frame recorded by the CCD camera of an ethylene/air diffusion flame established over the burner surface is displayed in Fig. 2(a). The flame location corresponds to the lighter layer and the soot to the darker region between the flame and the burner surface. It can be observed that the flame follows a boundary layer pattern, and that the soot layer grows in thickness with the distance from the flame leading edge. Photographs of Fig. 2 are used for the extinction measurements presented in Fig. 2(b).

In the analysis of the data, Bouguer's law, along with the non-scattering assumption, leads to directly inferring the local absorption coefficient $a_\lambda(x,z)$ from the attenuation measurement $A_\lambda(x,z)$, which represents the extent of the light intensity i extinction along a path from 0 to L_y and parallel to the y axis. This is given by

$$a_\lambda(x,z) = -\frac{1}{L_y} A_\lambda(x,z) = -\frac{1}{L_y} log\left[\frac{i_\lambda(x,L_y,z)}{i_\lambda(x,0,z)}\right] \quad (1)$$

where L_y is the absorbing path, *i.e.* the flame width here. By resorting to the Mie's theory in the Rayleigh's limit, the soot volume fraction $f_{soot}(x,z)$ can be inferred from:

$$\frac{a_\lambda(x,z)}{f_{soot}(x,z)} = \frac{36\, n_\lambda^2\, \kappa_\lambda\, \pi}{\left[n_\lambda^2\left(1-\kappa_\lambda^2\right)+2\right]^2 + 4\, n_\lambda^4\, \kappa_\lambda^2}\, \frac{1}{\lambda} \quad (2)$$

where n_λ and κ_λ are respectively the real and the imaginary parts of the refractive index at the considered wavelength. For the present study, Habib and Vervisch's indexes (Habib and Vervisch, 1988) were selected.

Figure 3 shows side views of a visible “open-tip” flame and its grey image for a fixed ethylene injection velocity of V_F=6.4mm/s and for three oxidizer velocities. For this example,

the oxidizer is composed of 21% O_2 and 79% N_2, but the observed trends are similar for other O_2 concentrations. To generate the grey images of the figure an intensity threshold in the CCD camera output is established to define a binary image and to differentiate the blue (white) from the yellow regions (black). It is seen that as the oxidizer velocity is increased the flame approaches the surface, becomes longer and increases in luminosity. This result is in contrast with that observed with flames at higher oxidizer velocity and/or oxygen concentration where the flame length and luminous intensity follow the reverse trend. The present flames are “open-tip”, thus quench near the trailing edge. It has been shown that an increase in the flow velocity results in an increase in the trailing edge flame temperature. Consequently the quenching of the trailing edge occurs further downstream (Torero et al., 2002) and the flame length increases. For “close-tip” flames the process is reversed because the fuel is consumed earlier, eventually at large flow velocities, the cooling of the reaction at the leading edge and the reduced residence time will result in blow-off. This result is important because it seems to indicate the presence of a maximum in the flame length and luminosity at oxidizer velocities below those encountered in natural convection. Such a maximum has been observed for opposed flame spread (Olson, 1991) and the present results suggest that a maximum may be also present for co-current flame spread since its propagation is strongly dependent on the flame length.

The result would have implications for fire safety in spacecrafts since the ambient gas velocities are below those observed in natural convection, and longer and more luminous flames and faster co-current flame spread would represent a higher hazard. The increased brightness is more difficult to explain because visible flame shapes alone are not sufficient to evaluate sooting trends (Lin et al, 1999; Konsur et al. 1999). The transition between the blue and yellow (soot glowing) zones seems mostly insensitive to the airflow velocity, with only a very minor displacement upstream observed. A more detailed analysis, beyond the scope of

this work, is necessary to describe the relationship between the colour change and soot concentrations.

A systematic study of the flame emission and soot volume fractions was also conducted for different fuel and oxidizer velocities. The range of velocities studied is consistent with those where Vietoris et al. (2000) and Brahmi et al. (2005) observed an increase in the intensity of the visible flame. They named this region as the transitional region between blue and yellow flames, and correspond to a soot oxidation region.

A series of representative values of light emissions are presented in Fig. 2(b) for a specific streamwise location (x=25mm). This region is in the vicinity of the origin of the "yellow" zone. The measurements were conducted at λ=532nm, because at this wave-length the emission of the flame is mainly attributed to soot oxidation (Kennedy, 1997). It can be seen that light emissions increase with the oxidizer flow velocity. Being cautious about extrapolation, because sooting behaviour is highly system dependent in microgravity (Urban et al., 2000), these results seem to be in agreement with experiments conducted on axisymmetric burners.

Because of the enhancement of convection, it can be hypothesized that the oxidizer streamlines penetrate deeper into the fuel region, resulting in enhanced soot oxidation and thus increased intensity and the observed colour shift towards the "yellow". These observations indicate that global residence times might not be sufficient to describe the outcome of the soot formation and oxidation competition in diffusion flames, and that the local characteristic times need to be defined. Urban et al. (1998) has previously used this approach to show that the ratio of soot formation/soot oxidation characteristic times is larger for buoyant than for non-buoyant flames while the global residence time is smaller. A similar argument can be applied in this case.

Numerical simulation

It is of interest to provide a theoretical verification of some of the above experimental results. Analytical solutions based on the scaling analysis proposed by Urban et al. (1998) have been shown to result in good predictions for the shape of non-buoyant laminar jet diffusion flames in an air co-flow (Lin el al., 1999). However, significant discrepancies are observed when comparing predicted and experimental flame geometry close to the nozzle exit. This seems to indicate that a numerical model is required to properly define the characteristic soot related residence times and to analyze the effects of the flow field on soot trajectories for the present problem, which are the objectives of the present theoretical analysis.

The code used for the present simulations is a variant of the Fire Dynamics Simulator (McGrattan, 2004). The model is based on an approximated expression of the Navier Stokes equations where acoustic waves are filtered while still allowing large density and temperature changes (low Mach number approximation). Characteristic velocities and dimensions corresponding to this study preclude the use of the subgrid model included in this code, thus Direct Numerical Simulation (DNS) is used. The Radiative Transfer Equation, in its non-scattering approximation, is solved through a wide band model. As soot is not modeled in this code, the non-scattering approximation is appropriate. A narrow-band model that accounts for the two main combustion products, H_2O and CO_2, computes the absorption coefficients required for each wide band. Details of the numerical tool and the modifications incorporated are presented in Rouvreau et al. (2002) and McGrattan (2004).

Although the combustion chemistry is expected to be complex for the present problem, the heat release is the only influence of the chemical reaction on the aerodynamics of the flow, which is a primary objective of this analysis. The region of interest is away from the trailing edge thus in this region the Damköhler number is expected to be large, and with fast chemical

kinetics. In contrast, finite kinetics would be required to model the extinction process at the trailing edge of the flame and consequently the flame length (Legros et al., 2005). Since the primary objective of this study is to analyze the effects of the flow field on the soot trajectories, it is only necessary to reproduce temperature field. Therefore, only a global one-step reaction, governed by an Arrhenius law with the constants proposed by Westbrook and Dryer (1981), has been used in the computations to simulate the ethylene combustion. To calculate the soot trajectory will be assumed that soot particles follow the streamlines. Although soot particles experience thermophoretic forces, the thermophoretic velocity is one order of magnitude lower than the convective velocities studied here (Konsur et al., 1999b; Sunderland et al., 1994a; Sunderland et al., 1994b). Therefore, thermophoretic effects are considered negligible here.

The dimensions of the computation domain and boundary conditions have been set to conform as much as possible to the experimental configuration (Legros et al., 2006). Figure 4 presents a schematic of calculation domain. This domain is 300mm x 200mm x 150mm in the x, y and z directions respectively. The regular Eulerian grid contains 120x80x60 grid cells, which gives a cell size of 2.5mm in each direction. This cell size has been chosen after checking that a reduction of the cell size (1mm, 0.5mm) does not lead to any significant differences in the results. Also, it has been checked that the results were independent of an increase of the domain size in any direction.

A flow of the oxidizer mixture at 305K and ambient pressure is imposed on the plane x=-50mm. The flat plate that holds the burner covers the whole plane z=0. The porous burner is embedded in the plane z=0, centred in the y direction and at 50mm from the inlet of the domain. A no-slip and adiabatic conditions are imposed on this boundary. An adiabatic boundary condition for the plate, although not realistic, has been chosen for simplicity. The influence of heat loss at the burner surface is not believed to be of major significance for the

present study. The boundary conditions at the four other sides of the domain $x=X_{max}$=250mm, y=0, $y=Y_{max}$=200mm and $z=Z_{max}$=150mm, are that of a passive opening, i.e., zero velocity and temperature gradients. Gravitational acceleration is set to zero.

The code was modified so that fictitious particles could be injected through the porous square burner. The particles have no mass, therefore follow the gas phase flow lines and have the gas temperature. Given the typical diameter of a soot particle (~50nm), the time lag for the soot temperature to rise to the gas temperature is much smaller than the residence time. At each time step, the particle position is tracked, together with its velocity and its temperature. The results presented here correspond to those after the flow has reached steady-state conditions.

Numerical results and discussion

A series of computations of the gas/soot temperature and gas flow field were carried out for different fuel and oxidizer velocities. Trends were unaffected by the fuel velocity so a single case (V_F=6.4mm/s) will be used to illustrate the results. Three oxidizer velocities (V_{ox}=150, 200, 250mm/s) corresponding to the experiments will be discussed. All the following numerical results will be related to the symmetrical plan (y=100mm) since this diffusion flame has been shown to be highly two-dimensional (Legros et al., 2006).

Figure 5 shows the temperature history of particles injected at t=9s, when steady state conditions had been attained. Figure 5(a) represents a particle injected close to the burner leading edge (x=11.25mm) and Figure 5(b) one injected close to the burner trailing edge (x=36.25mm). The end of the traces represents the time when the particles have reached the end of the computational domain. For the particle introduced at x=11.25mm, (Fig. 5(a)) the results show that the oxidizer velocity has a minor effect on the temperature rise of the particle, although an increase in velocity accelerates the temperature rise. Within 10 seconds

the particle has almost linearly increased in temperature to a peak of approximately 420^{o}C. Once this peak has been reached the temperature remains almost constant until the particle leaves the domain. The time scales for the particle introduced at the porous square trailing edge are similar but the peak temperature is approximately 120^{o}C lower (Fig. 5(b)). After this initial peak has been reached the particles continue to increase in temperature but at a much smaller rate. The initial peak is only weakly influenced by velocity, but the secondary rate increases significantly with the oxidizer flow.

Particles can only be injected from the fuel surface, thus the injection locations only represent a boundary for the soot inception region. The work of Kennedy (1997) indicates that at the calculated peak temperature of 420°C the soot formation process can start. Fuel will diffuse towards the flame continuing the generation of soot, therefore it is important to also illustrate this region. In Fig. 6(a) the maxima of temperature in the flame are traced for different oxidizer velocities as a function of the streamwise coordinate x. The flame reaches the peak in the zone of the porous square between 1400°C and 1600°C. This temperature confirms that the soot formation process occurs (Glassman, 1998). Figure 6(b) presents the upstream particle trajectory (injected at x=11.25mm) together with the locus of the maximum gas temperature (numerical flame location). It can be seen that as the oxidizer velocity increases, both particle and flame get closer to the surface, with the relative distance between particles and flame remaining approximately the same. Figure 6(b) also presents the location of the initial temperature peak for the different velocities studied. It can be seen that after the particle has reached its peak temperature it travels almost parallel to the flame explaining the constant temperature zone. For the higher velocities, the particles seem to deviate slightly towards the flame, which explains the slight temperature increase observed in Fig. 5(a) (t>12s). The peak temperature approaches slightly the leading edge of the burner as the

oxidizer velocity increases. This is consistent with the visual observations of Fig. 2 that show an upstream displacement of the “yellow” zone.

Calculated vertical velocity fields are presented for V_{ox}=150 mm/s (see Fig. 7(a)) and V_{ox}=250 mm/s (see Fig. 7(b)). The solid lines represent the streamlines and the dashed lines are the maximum temperature location. The two streamlines, coming out from x=0mm and x=50mm, are the fuel flow boundaries. The region within these two streamlines is thus the area where most likely soot will be formed and oxidized. The streamlines of oxidizer cross the flame entering the fuel zone and then are rapidly expelled again. For both flow velocities, the entries of the streamlines occur for x<120mm, which is consistent with the blue zone in the visual observations of Fig. 3.

At the leading edge of the burner there is a region of negative vertical velocity close to the surface, and above this region there is a zone where the flow is strongly accelerated. Rouvreau et al. (2002) discussed this flow feature in detail in a previous study. Figure 7(a) shows that for low velocities this region is characterized by a long residence time and significant separation from the flame, thus lower temperatures. In contrast, for higher velocities the residence time is shorter but temperatures are higher. The effect of the flow velocity seems to scale-up as the magnitude of the oxidizer flow increases in a manner that the ratio of soot formation to oxidation residence times remains fundamentally constant. This contradicts the observed increasing trend of the soot volume fraction with oxidizer flow (see Fig. 2). Closer observation of Fig. 7 shows that the only drastic difference between the two cases is a strong increase in the vertical velocity close to the flame region. This is also evident in Fig. 5(b) and Fig. 6. The increased magnitude of the vertical velocity will force soot particles to traverse the high temperature region much faster, thus reducing the soot oxidation residence time. This will lead to an increase in the peak soot volume fraction with the oxidizer flow velocity as observed in Fig. 2.

The numerical computations performed in this study appear consistent with earlier studies conducted on axisymmetric burners (Lin et al., 1999; Lin and Faeth, 1999).

Conclusions

A combined numerical and experimental study was conducted with laminar, flat plate boundary layer ethylene diffusion flames at low velocity, microgravity oxidizer flows. It was shown that despite shorter global residence times, an increase in oxidizer flow velocity results in an increase in local soot volume fractions as well as increased rates of oxidation, as evidenced by more intense glowing. It was also observed that the flames become longer as the flow velocity is increased in contrast with the reversed trend observed in flames at higher flow velocities. This result is important because it seems to indicate the presence of a maximum in the flame length and luminosity at oxidizer velocities below those encountered in natural convection. The result would have implications for fire safety in spacecrafts since the ambient gas velocities are below those observed in natural convection, and longer and more luminous flames represent a higher hazard.

It was also established that the ratio of the soot formation characteristic time to the soot oxidation characteristic time in the flame increases with the oxidizer velocity due mainly to a strong acceleration of the oxidizer flow external to the flame. The acceleration results in shorter residence times for soot oxidation, thus in an ultimate increase in the soot volume fraction.

Acknowledgements

This work was funded by CNES and ESA. Parabolic flights campaigns took place on board the Novespace A300-zeroG.

References

Brahmi, L., Vietoris, T., Rouvreau, S., Joulain, P., David, L. and Torero, J.L. (2005), Microgravity Laminar Diffusion Flame in a Perpendicular Fuel and Oxidizer Stream configuration, *AIAA Journal*, **43**, 1725.

Fernandez-Pello, A.C., Walther, D.C., Cordova, J.L., Steinhaus, T., Quintiere, J.G., Torero, J.L., and Ross, H. (2000), Test Method for Ranking Materials Flammability in Reduced Gravity, *Space Forum*, **6**, 237.

Glassman, I. (1998), Sooting Laminar Diffusion Flames: Effect of Dilution, Additives, Pressure, and Microgravity, *Proc. Combust. Inst.*, **28**, 1589.

Habib, Z.G. and Vervisch, P. (1988), On the Refractive Index of Soot at Flame Temperature *Combust. Sci. Technol.*, **59**, 261.

Kennedy, I.M. (1997), Models of Soot Formation and Oxidation*, Prog. Energy Combust. Sci.*, **23**, 95.

Konsur, B., Megaridis, C.M., and Griffin, D.W. (1999a), Fuel Preheat Effects on Soot-Field Structure in Laminar Gas Jet Diffusion Flames Burning in 0-g and 1-g, *Combust. Flame*, **116**, 334.

Konsur, B., Megaridis, C.M., and Griffin, D.W. (1999b), Soot Aerosol Properties in Laminar Soot-Emitting Microgravity Nonpremixed Flames, *Combust. Flame*, **118**, 509.

Legros, G., Fuentes, A., Rollin, B., Joulain, P., Vantelon, J.P., and Torero, J.L. (2005), Extinction Simulation of a Diffusion Flame Established in Microgravity, *Proc. of the 4th ICCHMT,* **1**, 560.

Legros, G., Joulain, P., Vantelon, J.P., Fuentes, A., and Torero, J.L. (2006), Soot Volume Fraction Measurements in a Three Dimensional Laminar Diffusion Flame Established in Microgravity, *Combust. Sci. Technol,* **178** (4), In Press.

Lin, K.C. and Faeth, G.M. (1999), Shapes of Nonbuoyant Round Luminous Laminar-Jet Diffusion Flames in Coflowing Air, *AIAA Journal*, **37**, 759.

Lin, K.C., Faeth, G.M., Sunderland, P.B., Urban, D.L., and Yuan, Z.G. (1999), Shapes of Nonbuoyant Round Luminous Hydrocarbon/Air Laminar Jet Diffusion Flames, *Combust. Flame*, **116**, 415.

Markstein, G.H. and De Ris, J. (1984), Radiant Emission and Absorption by Laminar Ethylene and Propylene Diffusion Flames, *Proc. Combust. Inst.*, **20**, 1083.

McGrattan, K. (2004), Fire Dynamics Simulator V4, Technical Reference Guide, NIST Special Publication.

Megaridis, C.M., Konsur, B., and Griffin, D.W. (1996), Soot-Field Structure in Laminar Soot-Emitting Microgravity Nonpremixed Flames, *Proc. Combust. Inst.*, **26**, 1291.

Mortazavi, S., Sunderland, P.B., Jurng, J., Köylü, Ü.Ö., and Faeth, G.M. (1993), Structure of Soot-Containing Laminar Jet Diffusion Flames, *AIAA paper*, 93-0708.

Olson, S.L. (1991), Mechanisms of Microgravity Flame Spread over a Thin Solid Fuel: Oxygen and Opposed Flow Effects, *Combust. Sci. Technol.*, **76**, 233.

Olson, S.L. and T'ien, J.S. (2000), Buoyant Low-Stretch Diffusion Flames beneath Cylindrical PMMA Samples, *Combust. Flame*, **121**, 439.

Rouvreau, S., Joulain, P., Wang, H.Y., Cordeiro, P., and Torero, J.L. (2002), Numerical Evaluation of Boundary Layer Assumptions Used for the Prediction of the Stand-off Distance of a Laminar Diffusion Flame, *Proc. Combust. Inst.*, **29**, 2527.

Sunderland, P.B., Mortazavi, S., Faeth, G.M., and Urban, D.L. (1994a), Laminar Smoke-Points of Nonbuoyant Jet Diffusion Flames, *Combust. Flame*, **96**, 97.

Sunderland, P.B., Köylü, Ü.Ö, and Faeth, G.M. (1994b), Soot Formation in Weakly Buoyant Acetylene-Fueled Laminar Jet Diffusion Flames Burning in Air, *Combust. Flame*, **100**, 310.

Torero, J.L., Vietoris, T., Legros, G., and Joulain, P. (2002), Estimation of a Total Mass Transfer Number from the Stand-Off Distance of a Spreading Flame, *Combust. Sci. Technol.*, **174**, 187.

Urban, D.L., Yuan, Z.G., Sunderland, P.B., Lin, K.-C., Dai, K., Faeth, G.M. (2000), Smoke-Point Properties of Non-Buoyant Round Laminar Jet Diffusion Flames, *Proc. Combust. Inst.*, **28**, 1965.

Urban, D.L., Yuan, Z.-G., Sunderland, P.B., Linteris, G.T., Voss, J.E., Lin, K.C., Dai, Z., Sun, K., and Faeth, G.M. (1998), Structure and Soot Properties of Nonbuoyant Ethylene/Air Laminar Jet Diffusion Flames, *AIAA Journal*, **36**, 1346.

Vietoris, T., Ellzey, J.L., Joulain, P., Mehta, S.N., and Torero, J.L. (2000), Laminar Diffusion Flame in Microgravity: the Results of the MiniTexus 6 Sounding Rocket Experiment, *Proc. Combust. Inst.*, **28**, 2883.

Westbrook, C.K. and Dryer F.L. (1981), Simplified Reaction Mechanisms for the Oxidation of Hydrocarbon Fuels in Flames*, Comb. Science and Technol.*, **27**, 31.

Xu, F., Dai, Z., and Faeth, G.M. (2002), Flame and Soot Boundaries of Laminar Jet Diffusion Flames, *AIAA Journal*, **40**, 2439.

List of figure captions

Figure 1. Schematic of the combustion chamber and burner

Figure 2. Measurements of light attenuation through the flame (a), leading to the cross-section (b) at x=25mm, plotting soot volume fraction versus z coordinate for different oxidizer velocities and a fuel velocity of V_F =6.4mm/s [18].

Figure 3. Flame side views on the left and corresponding grey pictures (intensity threshold of 150 a.u.(black)) on the right. All flames correspond to V_F=6.4mm/s and: (a) V_{ox}=150mm/s, (b) V_{ox}=200mm/s, (c) V_{ox}=250mm/s.

Figure 4. Schematic of the calculation domain.

Figure 5. Temperature time history for particles injected at: (a) x=11.25mm; (b) x=36.25mm.

Figure 6. (a) Maxima of temperature in the flame and (b) pathlines of particles injected at x=11.25mm and maxima of temperature locations, both as a function of the streamwise coordinate x for different oxidizer velocities.

Figure 7. Map of vertical velocity in the flame for: (a) V_{ox}=150mm/s; (b) V_{ox}=250mm/s. Solid lines are streamlines of oxidizer and dashed lines are the maximum temperature along the x axis.

List of figures

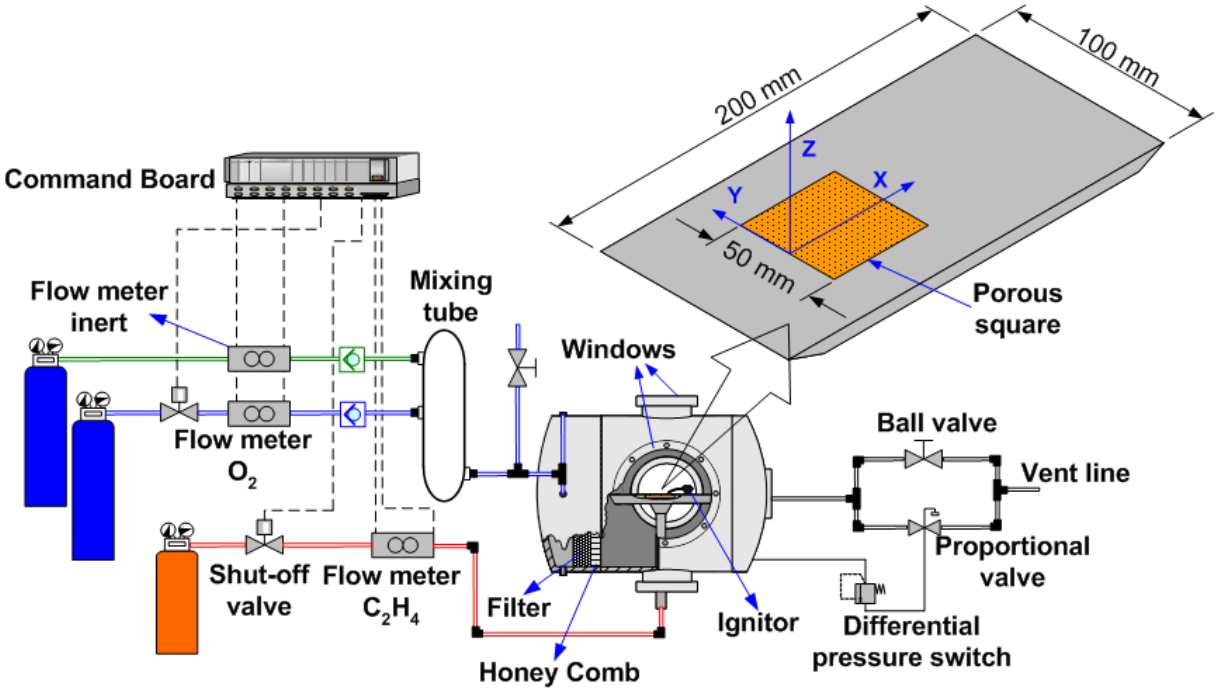

Fig. 1

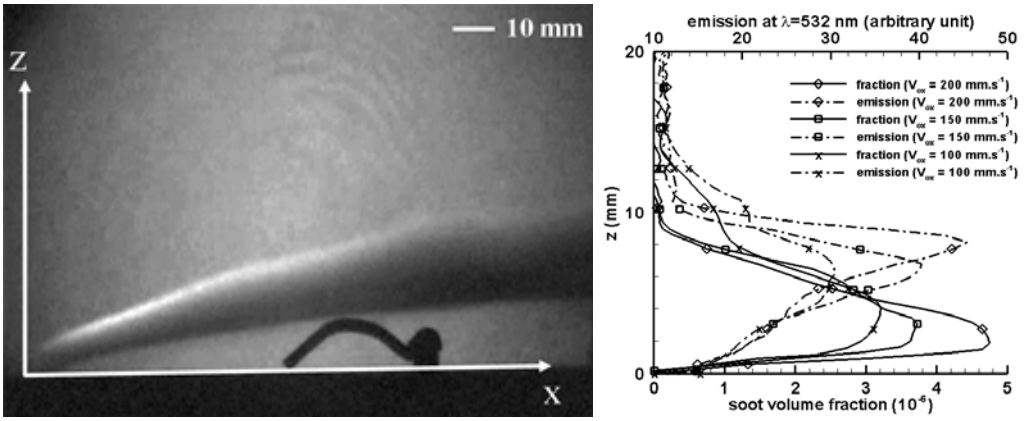
10 mm
Z
X
emission at λ=532 nm (arbitrary unit)
10
20
30
40
50
20
10
0
z (mm)
fraction (V_ox = 200 mm.s-1)
emission (V_ox = 200 mm.s-1)
fraction (V_ox = 150 mm.s-1)
emission (V_ox = 150 mm.s-1)
fraction (V_ox = 100 mm.s-1)
emission (V_ox = 100 mm.s-1)
0
1
2
3
4
5
soot volume fraction (10-6)

(a) **(b)**

Fig. 2

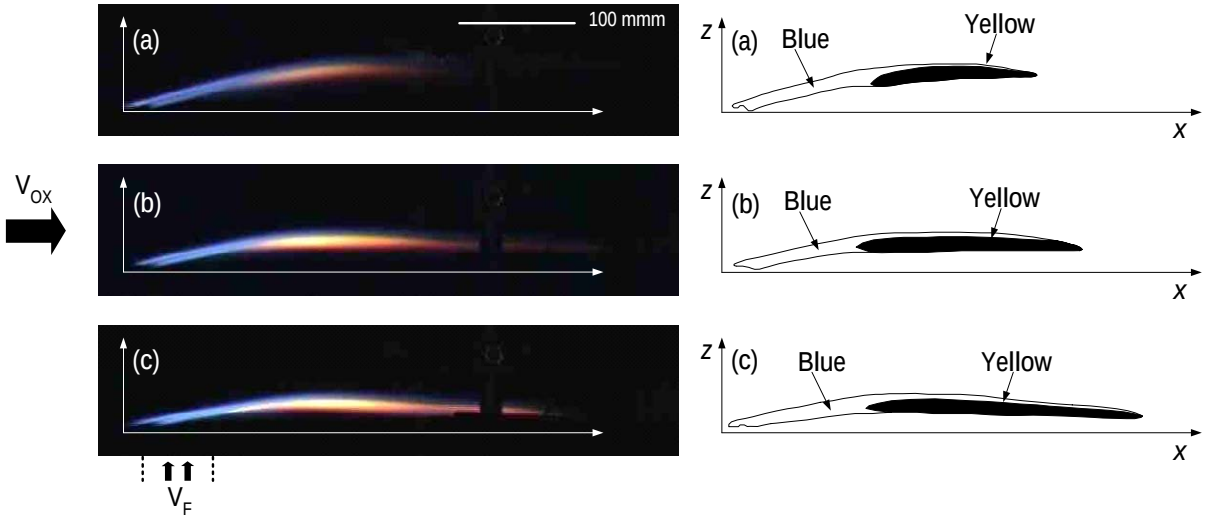

Fig. 3

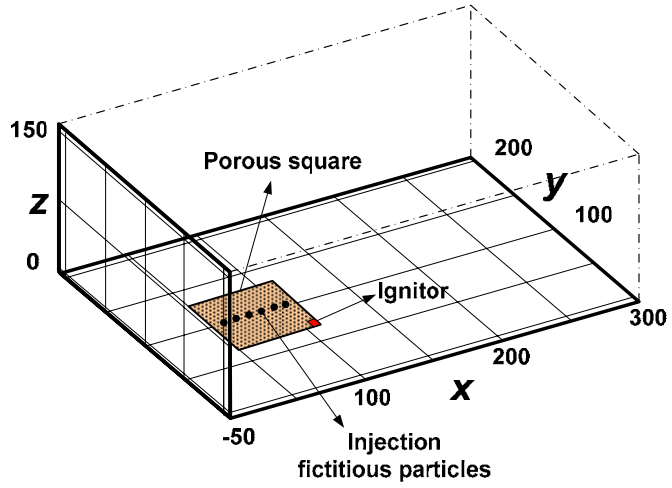
150
z
0
Porous square
200
y
100
Ignitor
300
200
100
x
-50
Injection
fictitious particles

Fig. 4

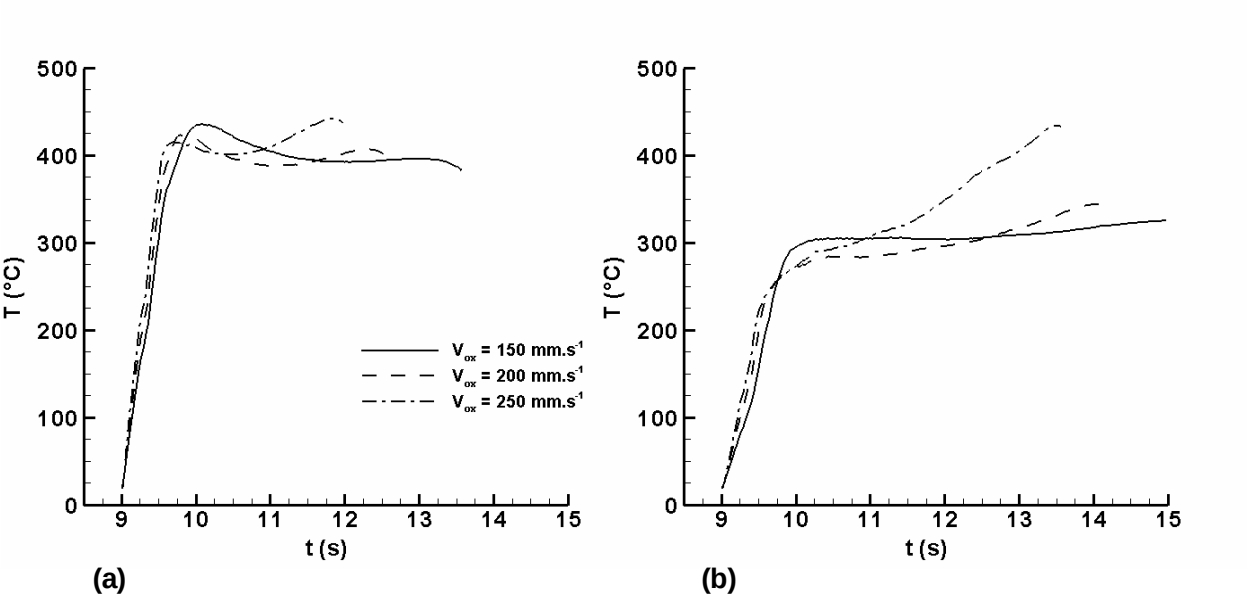

Fig. 5

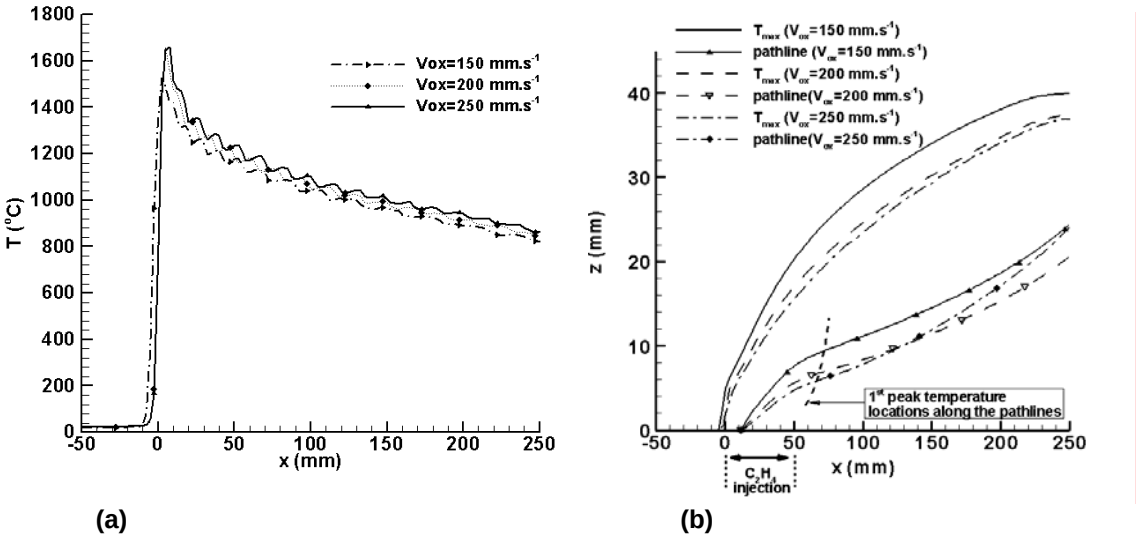
T (°C)
x (mm)
Vox=150 mm.s-1
Vox=200 mm.s-1
Vox=250 mm.s-1
(a)
z (mm)
x (mm)
Tmax (Vox=150 mm.s-1)
pathline (Vox=150 mm.s-1)
Tmax (Vox=200 mm.s-1)
pathline(Vox=200 mm.s-1)
Tmax (Vox=250 mm.s-1)
pathline(Vox=250 mm.s-1)
1st peak temperature locations along the pathlines
C2H4 injection
(b)

Fig. 6

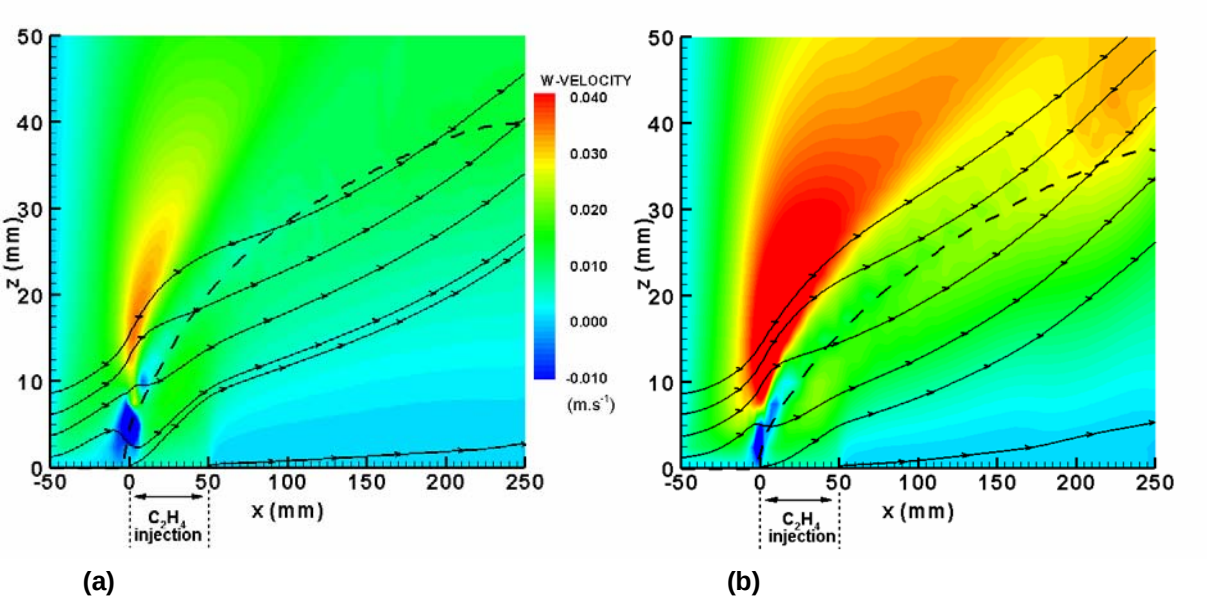
W-VELOCITY
0.040
0.030
0.020
0.010
0.000
-0.010
(m.s-1)
z (mm)
x (mm)
C2H4 injection
(a)
(b)

Fig. 7